J Mater Sci (2008) 43:5143–5156
DOI 10.1007/s10853-008-2727-6

An investigation of the structure–property relationships in melt-processable high-acrylonitrile copolymer filaments

Shawn R. Hutchinson · Alan E. Tonelli · Buphender S. Gupta · David R. Buchanan

Received: 25 January 2008 / Accepted: 14 May 2008 / Published online: 7 June 2008

Abstract A comprehensive investigation was undertaken to understand why the structure of a high-acrylonitrile (AN) resin renders it melt processable, how it affects the microstructure, and what filament properties it supports. High-AN homo- and copolymers have excellent chemical and ultraviolet light resistances that make them suited for many engineered industrial applications. Traditionally, these AN-copolymers are dissolved in a solvent and extruded into fibers by dry and wet spinning, because they tend to degrade rather than melt. Recent advances in copolymer synthesis have created the first AN-resins that can be melt processed, and, are produced more economically and in an environmentally friendly way. The block distributions were examined using solution nuclear magnetic resonance. Thermal behavior of the solid-to-ductile transitions was observed with differential scanning calorimetry to gain insight into the nature of the temperature-dependent solid-state interactions between chains. Filament extrusion was conducted utilizing a range of parameters to obtain filaments varying in structures and properties. Wide-angle X-ray diffraction was used to gain insight into the solid-state conformations and organization of the copolymer chains. It is concluded that melt-extruded filaments do not develop a distinct semi-crystalline morphology, but instead tend to develop a paracrystalline ordered structure. Mechanical properties can be varied, and under optimal conditions, compare favorably with those found in other melt-extruded polymer fibers that are not, resistant to chemical and UV exposure.

S. R. Hutchinson (✉) · A. E. Tonelli · B. S. Gupta · D. R. Buchanan
College of Textiles, North Carolina State University, Box 8301, 2401 Research Drive, Raleigh, NC 27695-8301, USA
e-mail: shawn.hutchinson@gmail.com

Introduction

Acrylonitrile (AN) homo- and copolymers, or Acrylics, are recognized as an inexpensive choice for fiber applications requiring resistance to chemical and ultraviolet exposure. However, the nature of their microstructures required that homo- and copolymers be dissolved in a solvent and extruded by the less desirable wet or dry spinning technologies [1]. Because of this environmentally unfriendly and more expensive technology, the applications of acrylic have declined, and are currently well below those possible if they were melt extrudable. As copolymerization of acrylics can include a range of comonomers, AN-copolymers offer more attractive engineering properties for specific applications. New affordable applications of 'melt'-processable acrylics could create new plastics for membranes, space exploration, and carbon fiber applications.

Before research and development of new engineered applications from melt-processable high-acrylonitrile copolymers (MPHAC) can commence, a clear understanding of what makes these new acrylics and their properties different is necessary. Because of the high polarity of the cyano sidegroup in the AN repeat units, a comonomer, often methyl acrylate (MA) or vinyl acetate (VA), was included to improve the processability that was traditionally done in solution [2]. The resulting comonomer sequence structure is blocky, with a distribution that depends on the reactivity ratios of AN and the comonomer. Yet these copolymers were still only processable in solution, as they degraded at elevated temperatures [3]. Since copolymerization of acrylics can include many different comonomers, new opportunities for developing materials for new and attractive engineering applications are possible. However, little is known about the detailed microstructures of MPHAC polymers and the nature of the

structures and organizations, and resultant properties developed in their melt-extruded filaments.

In this study, the comonomer sequence distribution or block structure of the MPHAC-copolymers were examined utilizing ^{13}C Nuclear Magnetic Resonance (NMR), which provided a means to analyze the average lengths of consecutive AN sequences. Comonomer sequence or block length differences could explain the differences in thermal properties of these resins. Differential scanning calorimetry (DSC) thermograms, endotherms, and exotherms, were used to infer more specifically how the microstructure, organization of the resins differ from melt-extrudable semi-crystalline polymers and copolymers, such as polyamides and poly(ethylene terephthalate) in particular. Their melt-extruded filaments were subjected to different types and levels of drawing to influence fiber structure and resultant mechanical properties. Paracrystalline lattice structure and parameters were evaluated utilizing wide-angle X-ray diffraction (WAXS) procedures, which gave information regarding the topology and amount of paracrystalline order (PO). This proved useful in understanding the structure–property correlations that were developed in the melt-spun filaments. A WAXS transmission photograph was collected of a highly drawn filament to show a representation of the order present. Trends observed between the mechanical properties (tenacity, elongation, and initial modulus), the orientation, the PO, and the paracrystal sizes provided means to understand the relationships between the fiber microstructures and their properties.

Polyacrylonitrile (PAN) itself is a unique vinyl polymer, because of its chemical and UV resistances and paracrystalline morphology. Specifically, one of its most notable properties is the low thermal degradation range, 250–310 °C, which rendered acrylics processable only from solution [4]. For most thermoplastic polymers the relationship between crystalline morphology and melting point is well understood in terms of discrete crystalline and amorphous domains and as an equilibrium first-order thermodynamic phase transition [5]. However, PAN does not exhibit the classical two-phase morphology and has been described as paracrystalline [6], "amorphous with a high degree of lateral bonding," [1] or as a "two-dimensional liquid crystalline-like structure with many defects" [7]. Despite early conflicting conclusions about its tacticity as radically polymerized [8–11], which were later resolved [12], the degree of (para)crystallinity for the PAN homopolymer does not appear to be a strict function of stereoregularity [13]. Similar behavior is also observed in poly(vinyl alcohol), poly(vinyl chloride), and poly(norbornene) [14].

In general, to alter the crystal morphology and melting temperatures of homopolymers, comonomers are used to reduce the copolymer melting temperature. Theoretical work by Flory [15] and Eby [16] suggest microstructural control of copolymer melting temperatures. Flory asserts that comonomer interruption and shortening of the length of the crystallizable monomer sequences reduces the number and average size of crystallites. Because chain segments on the crystallite surfaces have larger free energy, smaller crystals with a larger surface-to-volume ratio have a reduced melting point [1]. Furthermore, for non-random copolymers, Flory proposed that the melting point depression depends on the comonomer sequence propagation probability, as well as the overall comonomer composition [17]. Eby, on the other hand, proposed that comonomers may be incorporated into the crystal lattice as defects and extended Flory's theory by adding a parameter that accounts for the degree of lattice disruption.

To date, the only reported way to affect the PAN 'melt' temperature is through free-radical copolymerization by controlling reaction parameters, including comonomer concentrations and reactivities. The enchainment of comonomers in the resulting copolymers is considered to be somewhat blocky, and not completely random [18]. A comonomer concentration over 15%, MA or VA creates a modified acrylic, or modacrylic, which at sufficiently high incorporation produces an amorphous glassy material. To the extent that the thermal properties are dependent upon the lengths of the consecutive acrylonitrile (AN) sequences, a melt-processable high PAN ($\geq$85% AN) is possible if the lengths of the AN sequence were controllable, such that they are long enough to impart sufficient (para)crystallinity for mechanical integrity, while keeping the melting point below the degradation range. This would support the proposal by Flory that in this non-random copolymer, the comonomer sequence propagation probability, which determines the average AN run length, controls the melt behavior. The (para)crystalline domains could, however, still include the comonomer as suggested by Eby [16] and Frushour [1] or affect the (para)crystalline dimensions.

Smierciak et al. [19] developed a novel 'starved' or 'scavenged' emulsion copolymerization reaction based on work by Dimitratos et al. [20]. Under extremely low feed rates, the copolymerization rate approaches a pseudo-steady value based on the availability of the comonomers and their addition rate, and the composition of the copolymer is similar to the comonomer feed concentrations. In the 1990s this was industrially developed into a group of inherently melt-processable high acrylonitrile (MPHAC) resins, based on olefinic comonomers, through reduction in the AN run lengths to enable 'melting' before thermal degradation.

In the solid state of AN homo- and copolymers, intermolecular interactions create order whose morphology deviates from those of well-behaved semi-crystalline

materials. Observed tenacities of PAN filaments were similar to normally crystalline polymers like nylon 66 and poly(ethylene terephthalate), but attributed to different causes. Tenacity in semi-crystalline polymer materials develops from chemical structure, chain alignment, packing, and hydrogen bonding. The dominant factor determining tenacity in PAN, however, seems to result from the severe interchain interactions between AN sidegroups, which, through bond rotation, 'kinks' the chain conformation [7, 11]. These interactions create a 'braced' structure, thereby loosely forming symmetrical rods 0.6 nm in diameter [21]. Longitudinal order is absent, Bohn et al. note, due to an irregular helical conformation [7]. The authors further asserted that laterally ordered polymers have properties intermediate to crystalline and amorphous materials, but unlike traditional two-phase semi-crystalline polymers. Axial periodicity was absent in single crystal and drawn lamellae, where stereoregularity was unknown, though likely atactic, and the degree of lateral order was high [6, 22–24]. Changes in the microstructures of bulk homopolymer samples with temperature were noted [2, 25], and for copolymers also with the size and concentration of the comonomer, as well as processing conditions [25–28].

To summarize, high-AN copolymers offer properties unique to vinyl polymers due to the strong dipole moment in the AN sidegroup. Solid-state properties seem to be the result of the interactions between sidegroups, whereby irregular conformations are created that yield atypical bulk behavior. Rather than melting, traditional PAN homopolymers and high-AN copolymers exhibit degradation properties atypical to polymers with traditional semi-crystalline morphologies. The intermolecular interactions of the strong $-C\equiv N$ dipole moments leads to an irregular solid-state chain conformation regardless of their tacticity or stereoblock configurations. The laterally ordered regions likely pack in rods comprised by chains with helical conformations. Measurement and characterization of (para)crystallinity in the solid state, show attributes that vary with the processing parameters and comonomer particulars, like volume and concentration.

Materials and methods

Acrylonitrile copolymer

One version of a melt-processable high-acrylonitrile copolymer (MPHAC) was used. The pelletized copolymer resins were synthesized by British Petroleum and consisted of approximately 85/15 AN/MA with a number average molecular weight of 50,000 Da. A number average block sequence length of 13 for the AN comonomer was determined by ^{13}C-NMR with a Varian 300 NMR spectrometer. Tacticity was determined from the AN methine carbon region, as specified by Minagawa [13], which is atactic with approximately 52% m and 48% r diads.

Reference solution-spun acrylic fibers used for comparison were Dralon® and Orlon®. Dralon® type 251 bright 1.3 dtex of 95% AN: 5% MA was supplied by Dralon GmbH, Dormagen, Germany. Orlon® type 42 dull, once produced by DuPont, was used.

Extrusion

Filaments were extruded using a single-bore capillary device from Bradford University Instruments, Ltd. Pellets were dried under vacuum for 2 days at 120 °C. The capillary die had a 2 mm diameter, 25 mm length, and 90° entrance angle. A throughput rate of 1.25 –mm s^{-1}, as measured by the speed of the piston, was used. The pellets were heated for approximately 5 min at an optimal 220 °C [29], and the piston pressure was equilibrated before fibers were collected. A heat shroud set to 145 °C was placed below the spinneret to increase the spin-draw zone before the extrudate stream solidified.

Filaments were passed over a winding godet roller to prevent slippage and wrapped multiple times around two draw rollers. The rollers were heated to 115 °C [29] and the filament was drawn to different ratios before collecting them in a bag using an aspirator. Various spin- and hot-draw ratios were used to obtain specimens covering a range of processing settings. The spin-draw conditions were varied by the speed of the first draw roller from 100 to 700 m s^{-1} and the hot-draw ratios imparted between heated feed and draw rollers ranged from 200 to 700 m s^{-1}. Filaments with a spin-draw velocity of 700 m s^{-1} could not be drawn further. Samples are grouped according to their spinning conditions (Table 1).

Table 1 Draw conditions and filament groups

Draw roll 1 (m s^{-1})	Draw roll 2 (m s^{-1})	Group
100	100	A1
100	200	B1
100	300	B2
100	400	B3
200	300	C1
200	500	C2
300	300	D1
500	500	D2
700	700	D3

Solution ^{13}C-NMR

^{13}C-NMR spectra were recorded at 75.4 MHz in d_6-dimethylsulfoxide at 90 °C, with a pulse delay time (d1) of 10 ms, collection time (at) of 2 ms, and pulse angle (pw) of 90° on a Varian spectrometer [13]. Actual sequence lengths in commercial high-PAN fibers were calculated using triad concentrations obtained by integration of NMR spectra (Fig. 1) [30].

Differential scanning calorimetry

A Perkin-Elmer Diamond 7 DSC instrument, calibrated with indium and zinc, was used to collect thermograms. Filament specimens were conditioned at 25 °C and 65% relative humidity. Approximately 2.5–3.5 mg of filament was sealed in aluminum pans for volatiles. All samples were heated and cooled twice in the scan range of 50–240 °C at 30 °C min^{-1}, because this faster rate produced distinguishable and reproducible peaks. To ensure a similar heat history, the enthalpies reported are for the second cycle. For selected samples, additional heating and cooling rates were also employed.

Wide-angle X-ray diffraction and α-orientation

Diffraction spectra and photographic transmission patterns were collected with nickel-filtered CuK$_\alpha$ radiation using an Omni Instruments diffractometer set at 30 kV and 20 mA. A scintillation counter with a 0.1-mm slit was used to collect the spectra from 10 to 35°. Paracrystalline orientation of the overlapping [110]/[200] planes was obtained for each sample by collecting spectra of the azimuthal angle ϕ from 5 to 360° [11]. Peak widths were corrected for instrumental broadening using a linear regression of half breadth angles as a function of peak placement from a spectrum of powered hexamethylenetetramine.

The PO, similar to the degree of order (DO), as proposed by Gupta et al. [31], was calculated slightly differently. We extended the previous method to accommodate different spectral shapes produced by different sample forms, i.e., powder, film, or fiber. Commercial fibers show an example of the location and variation in the amount of scatter (Fig. 2). Five Pearson VII curves were used to fit the spectra (Fig. 3), whose positions and order are explicitly correlated with the Miller Indices and unit cell dimensions reported in other earlier studies [23, 32, 33]. The root mean square error of the non-linear fit was less than 0.1% and represents an accurate means of fitting a WAXS spectrum for PAN fibers.

$$I(2\theta) = \frac{I_0}{\left(1 + 4\left(\frac{2\theta - 2\theta_0}{w}\right)\left(2^{\frac{1}{m}} - 1\right)\right)^m},$$

where 2θ is the spectrum angle in radians, $2\theta_0$ is the peak placement in radians, I_0 is the peak intensity in arbitrary units, w is the peak half-width in radians, and m is a scalar shape factor. Root mean square errors of less than 1% were obtained from the fit of non-linear least squares. To ensure that peak statistics are comparable between samples, the same shape factor value (m) was used for peaks representing order and scatter, i.e., 0.001 and 1, respectively, whose value appeared to be a best fit of the data.

The x- and y-unit cell dimensions were solved simultaneously using the orthorhombic crystal shape equation and

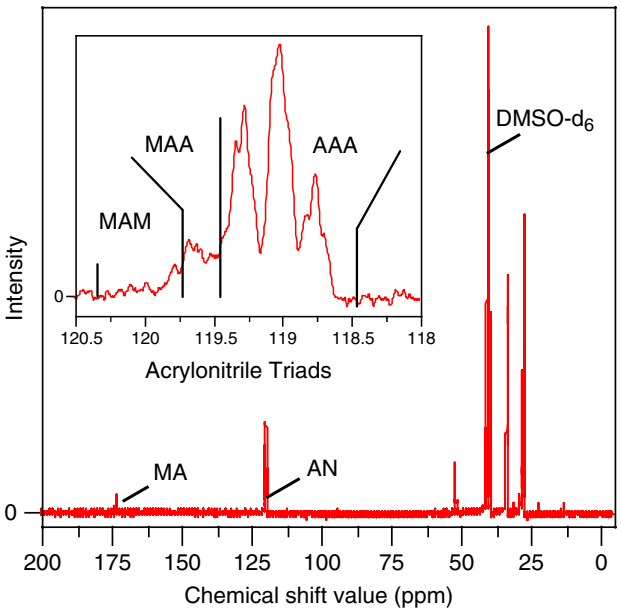

Fig. 1 ^{13}C-NMR solution spectrum of MPHAC

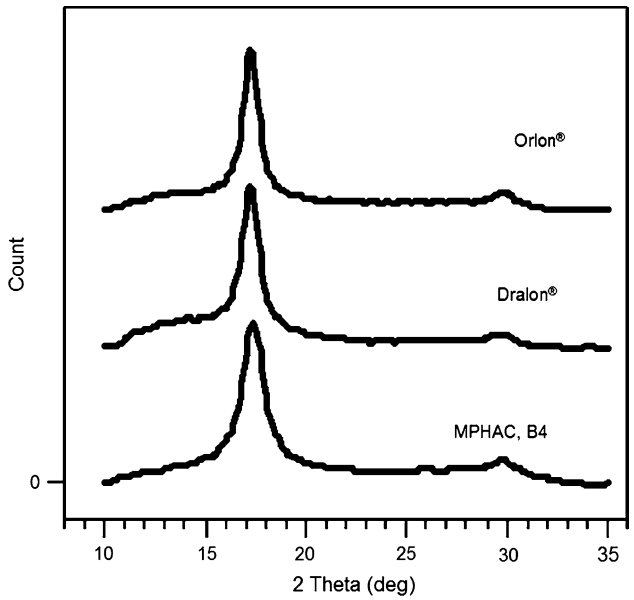

Fig. 2 WAXS diffraction spectra for acrylic fibers

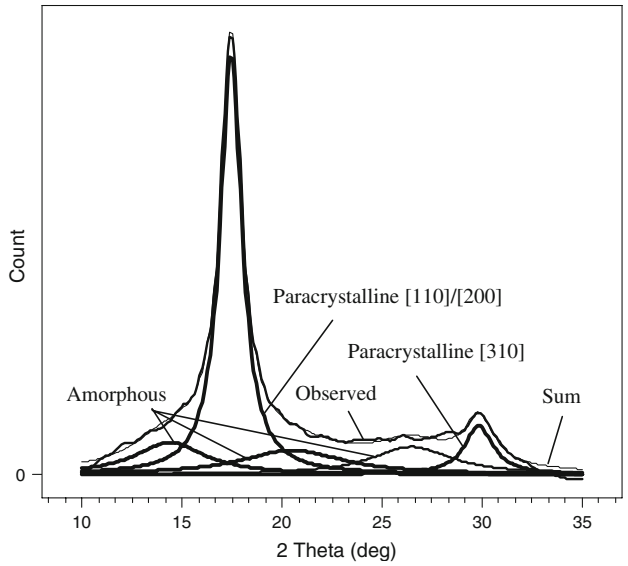

Fig. 3 Diffraction spectrum of MPHAC, B4 with non-linear least squares Pearson VII fits

the [110] and [310] lattice planes. *D*-spacing is thus calculated as:

$$d_{hk0} = \left(\left(\frac{a}{h}\right)^2 + \left(\frac{b}{k}\right)^2 \right)^{-\frac{1}{2}},$$

where *D*-spacing d_{hk0} is in nm, a and b unit cell dimensions in nm, and h and k are Miller Indices while 0 refers to two-dimensional paracrystalline order.

Paracrystal size was calculated using the Scherrer equation:

$$L_{hkl} = \frac{K\lambda}{\sqrt{\beta^2 - \gamma^2}},$$

where L_{hkl} is the paracrystal size in nm, K is a scalar geometric factor taken to be 0.9 in this instance, λ is the wave length of the CuK_α radiation in nm, β is breadth of peak at full-width half-maximum in degrees, and γ is the value of instrumental broadening correction function for the given peak placement in nm.

Paracrystalline orientation along the fiber axis was calculated using the Hermann orientation function. Azimuthal spectra were fitted using Pearson VII curves each having the same shape factor. Numerical integration was used to determine the average cosine square as a function of azimuthal angle ϕ:

$$\langle \cos^2 \phi \rangle = \frac{\int_0^{1.57} I(\phi) \cos^2 \phi \sin \phi d\phi}{\int_0^{1.57} I(\phi) \sin \phi d\phi}.$$

Hermann's orientation factor, f, was calculated using:

$$f = \frac{1}{2}\left(3\langle \cos^2 \phi \rangle - 1\right)$$

Sonic velocity, sonic modulus, and α-orientation

A Dynamic Modulus Tester DMT PPM-5R by Lawson-Hemphill was used to measure the sonic velocity along the filament axis. Filament specimens were conditioned at 25 °C and 65% relative humidity. Sonic modulus was calculated from measured sonic velocity using the following relation [34]:

$$E = 11.3C^2,$$

where E is the sonic modulus in cN dtex^{-1} and C is the sonic velocity in km s^{-1}. The molecular orientation was obtained via the acoustic or α-orientation function, proposed by Moseley:

$$\alpha = 1 - \frac{E_u}{E_o},$$

where α is a measure of orientation ranging from zero to unity, E_u is the sonic modulus of the unoriented material in cN dtex^{-1}, and E_o is the sonic modulus of the material in cN dtex^{-1}. The sonic modulus value used for the unoriented material was taken as 50.0 cN dtex^{-1} [35].

Mechanical properties

The filament samples were allowed to condition overnight at 25 °C and 65% relative humidity. The linear density and mechanical properties were measured on fibers with a gage length of 2.54 cm in accordance with the ASTM Standard 3288 using a Favimat, Textechno, Mödchengladbach, Germany, and a piston speed of 200 mm min^{-1}. Data for the force and elongation at break for ten specimens were collected for each filament. Draw ratio was determined from the ratio of the radius of the final filament to that of the capillary die, as no die swell was observed.

Size exclusion chromatography

A Waters 1525 binary high-pressure liquid chromatography pump with a Waters 2414 Refractive Index Detector was used to obtain chromatograms corresponding to the molecular weights of pellet and fiber samples. The column used was a single Polymer Labs PLgel, 5 μm particle size, mixed-d pore type, 300 × 7.5 mm^2 with a flow rate of 1 cm^3 min^{-1}. The column was heated to 50 °C and the detector was heated to 30 °C. A solution of 0.01 M LiBr-*N*,*N*-dimethyl formamide was prepared and used as the mobile phase [36]. Polytetrafluoroethylene syringe filters (1 μm pore size), solvent filters, and coated vials were used with all samples. Each standard was injected separately.

Results

Comonomer block structure

Since Flory's equation for melting point depression as a function of comonomer content, in combination with Eby's and Frushour's extensions, fails to fully predict the 'melting' behavior of AN-copolymers, another factor or factors must affect this behavior. Solution NMR has proved to be an insightful tool for understanding copolymer attributes not readily obtained from their bulk properties, especially comonomer run numbers. The predicted and observed number average AN sequence lengths, AN run number, of AN/MA (Fig. 4) and AN/VA copolymers with various compositions were compared. Flooded free-radical PAN comonomer sequence lengths are predicted from comonomer composition using the first-order Markov (Terminal) copolymerization model, comonomer reactivity ratios, and compared to those observed for free-radical AN/VA [37] and AN/MA copolymers [38] by Brar and Sunita. For MPHAC, the average length of contiguous AN units is approximately 13, which is over twice the flooded equivalent and ~3 times less than Dralon®. The resulting scavenged reaction-modified structures have block lengths of intermediate size, which may not be possible in a flooded copolymerization that yields an 85% AN:15% MA copolymer. Thus, the scavenged reaction may offer sequence control beyond that of the flooded comonomer reaction.

The number average AN sequence length in MPHAC is significantly shorter than a commercially available fiber and longer than modified acrylics. The sequence length itself lies above the theoretical predictions of the sequence length based on the first-order Markov model. Dralon® and Orlon®, which show longer sequence lengths, lie slightly above what is predicted by the theoretical model (~36).

Melt behavior

DSC thermograms show behaviors that are atypical compared with semi-crystalline polymers. While MPHAC thermograms are also sensitive to the heating rate, the shapes of the thermograms for the MPHAC copolymer are significantly different than those exhibiting a first-order thermodynamic phase transition (Fig. 5). Generally, thermograms for semi-crystalline polymers show distinct jumps and peaks, respectively, for glass and melting transitions. For MPHAC, rather than pronounced features appearing abruptly on the baseline, heat flow increases gradually with temperature showing inflections at the glass and 'melting' transitions. At a ramp rate of 20 °C min^{-1}, a slight endothermic peak is observed around 220 °C, but this is reduced to an inflection point at 10 °C min^{-1}. The magnitude of the glass transition inflection also increases with ramp rate. At a slower ramp rate of 5 °C min^{-1}, both inflections largely flatten into the baseline.

Cooling behavior

Cooling exotherms also show MPHAC behavior atypical of semi-crystalline polymers. Rather than a gradual increase in heat flow with temperature observed in the heating cycles, cooling exhibits a pronounced recrystallization peak (Fig. 6). The peak also gradually flattens toward the baseline with a decrease in cooling ramp rate.

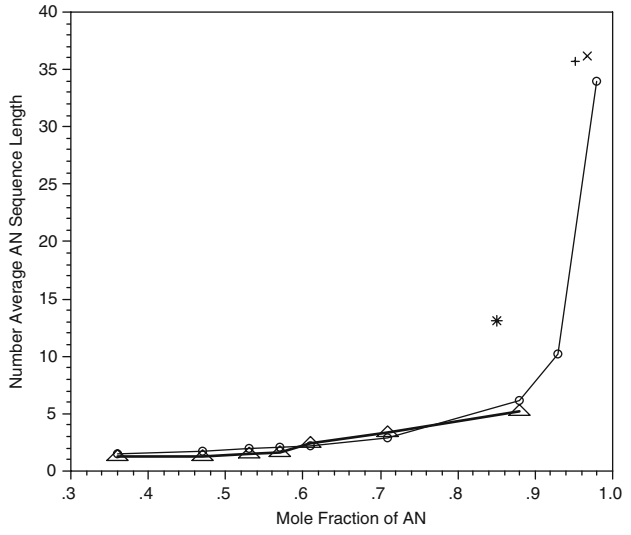

Fig. 4 First-order Markov predicted (○) and observed (△) [38] number average AN sequence lengths in AN copolymers, MPHAC (✳), Dralon® (+), and Orlon® (×)

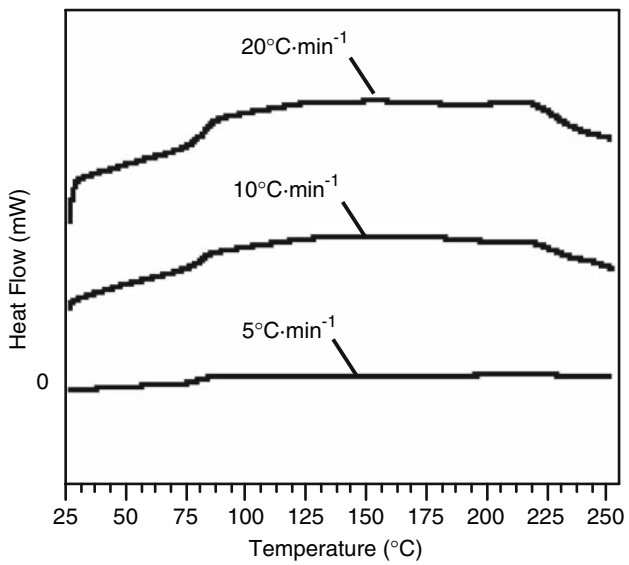

Fig. 5 DSC thermograms for MPHAC

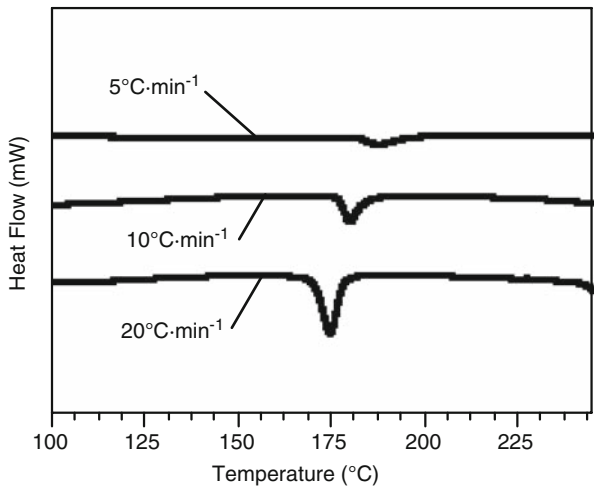

Fig. 6 DSC cooling thermograms for MPHAC

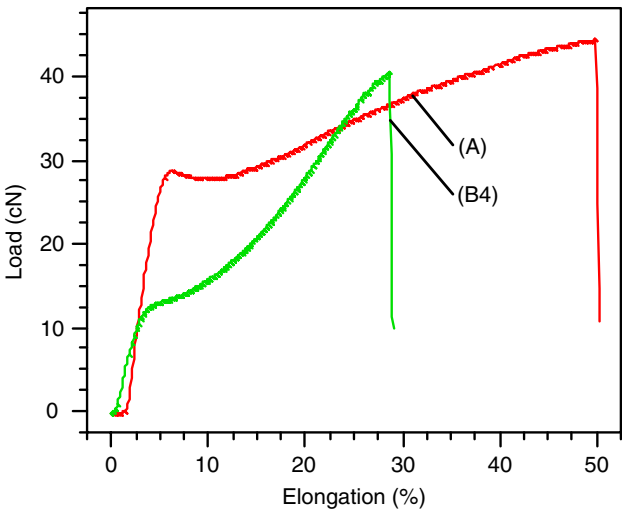

Fig. 7 Tensile curves for MPHAC filaments A and B4

Size exclusion chromatography

As mechanical properties are highly correlated with both molecular orientation and molecular weight, the molecular weights of filaments were determined and compared with those of the resin pellets. While the properties of MPHACs have been shown to be affected by processing, under proper processing conditions they maintain stability [29]. No significant changes in the molecular weight and distribution were observed for the MPHAC filaments (Table 2). The average polydispersity is 1.70 with a standard deviation of 0.03. Under appropriate conditions the molecular weight of MPHAC is shown not to be affected by processing.

Filament load elongation

Acrylic fiber and other fibers requiring solution processing exhibit deformation-strengthening behavior [39, 40]. In contrast, melt-processable polymers are expected to exhibit plastic deformation in a manner experienced with polymers such as polypropylene [41]. The MPHAC filament with the lowest draw exhibits plastic deformation behavior without the aid of steam or other plasticizing means (Fig. 7). Filaments with the lowest spin-draw ratio showing plastic deformation without a distinct necking zone and subsequently drew well with heat treatment. Those filaments spin- and hot-drawn further show deformation strengthening behavior that is typical of acrylic fibers.

Table 2 MPHAC molecular weight polydispersity

Draw roll 1 (m s^{-1})	Draw roll (1–2) (m s^{-1})	Polydispersity
Pellet		1.67
100	0	1.66
100	200	1.67
100	300	1.72
100	400	1.68
200	300	1.71
200	500	1.67
300	0	1.71
500	0	1.73
700	0	1.74

Paracrystalline order

An X-ray diffraction transmission photograph of MPHAC filament drawn with the highest hot-draw ratio shows pronounced arcs (Fig. 8). As observed in the diffraction spectrum, strong equatorial reflections are present. The main ordered peak at $2\theta \approx 17.3°$, corresponding to the [110]/[200] overlapped plane, is visible as the stronger arc [11]. The secondary ordered peak at $2\theta \approx 14.3°$, corresponding to a half reflection of the [310] plane and indexed

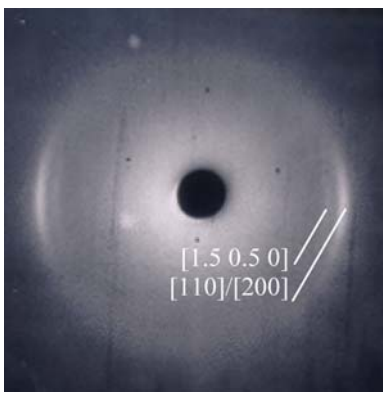

Fig. 8 WAXS transmission pattern for MPHAC filament B4

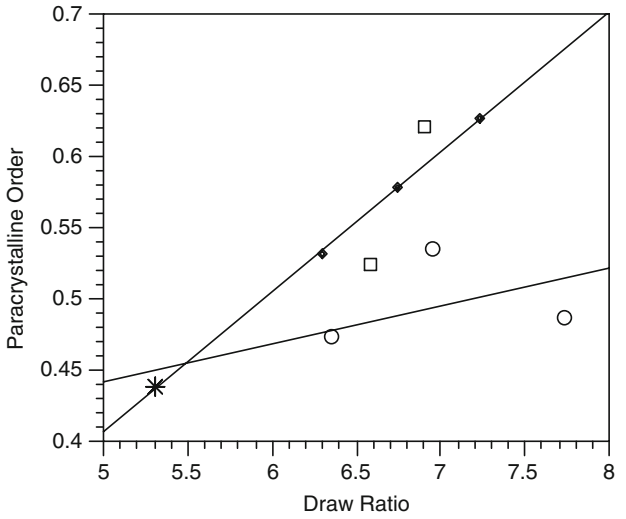

Fig. 9 PO by draw ratios. Filament groups (A) ✳, (B) ◆, (C) □ and (D) ○

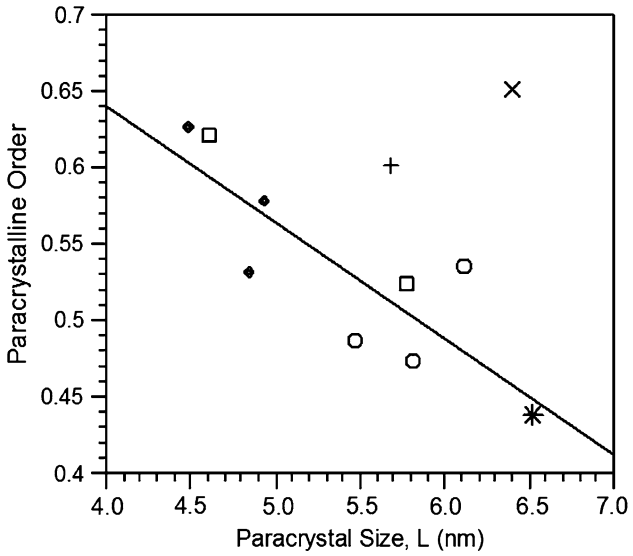

Fig. 10 PO and paracrystal Size. (A) ✳, (B) ◆, (C) □, (D) ○, Dralon® +, and Orlon® ×

as the [1.5 0.5 0] plane, is shown closer to the center with the fainter arc. Although the half-reflection arc is related to PO, it also appears in filaments under stress or tension, and since this peak arises from disordered regions it is tabulated as amorphous order. Concurrent with typical behavior of acrylics and unlike semi-crystalline polymers, no meridional reflections are apparent.

In most thermoplastic polymers, processing parameters affect their microstructures, from orientation to crystallinity [41]. For the filaments in the current study, the assessed PO was plotted as a function of total draw ratio that included both spin- and hot-draw (Fig. 9). Two linear regressions were fitted: one for filaments with only spin-draw and the other for filaments that also had hot-draw. The results show a strong relationship between PO and draw ratio, and in particular how the draw ratio is imparted. Filaments extruded with only spin-draw exhibit lower degrees of order, Groups A and D, and have an *R*-square linear fit value of 0.45 (Table 3). Filaments drawn with a low spin-draw and high hot-draw, Groups A and B, show a higher PO and an *R*-square linear fit value of 0.99. Thus, PO varies with extrusion conditions, and hot-drawing the filament results in the highest values of PO. With increasing paracrystal size, PO is shown to decrease (Fig. 10). By comparison, both Dralon and Orlon exhibit larger paracrystals sizes and higher values of PO, both of which are attributable to AN sequence lengths significantly longer than in MPHAC.

Unit cell parameters

The crystallography literature of high-AN homopolymers suggests that, due to the nature of the PO present, universal unit cell dimensions are evasive [11, 25, 32, 33]. Reported dimensions vary depending on the number and plane index observed, and with the form of the material, i.e., fiber, powder, or lamellae (Table 1). For the MPHAC-B4

Table 3 Mechanical properties and statistics of MPHAC-B4 filaments

Spin draw ratio, avg.	Hot draw ratio, avg.	Group	PO	Tenacity (cN dtex^{-1})	Std. Dev. (cN dtex^{-1})	Initial modulus (cN dtex^{-1})	Std. Dev. (cN dtex^{-1})	Elong. (%)	Std. Dev. (%)
5.31	0	A1	0.44	2.01	0.17	15.07	2.23	58.56	10.80
5.31	0.99	B1	0.53	3.77	0.44	32.82	4.60	29.34	3.25
5.31	1.44	B2	0.58	4.19	0.49	38.23	7.56	25.47	5.39
5.31	1.92	B3	0.63	5.15	0.68	54.16	5.95	25.00	11.12
5.94	0.63	C1	0.52	3.54	0.52	36.23	4.32	31.21	4.63
5.94	0.96	C2	0.62	3.85	0.56	41.64	6.05	23.52	1.80
6.36	0	D1	0.47	1.98	0.16	58.76	15.13	28.53	3.66
7.20	0	D2	0.54	2.75	0.20	41.30	9.73	21.09	1.00
7.73	0	D3	0.49	3.21	0.25	42.71	16.55	21.82	1.14

filaments, insignificant changes in cell dimensions were observed as a function of draw. The average dimensions are $a = 1.097 \pm 0.002$ nm and $b = 0.585 \pm 0.004$ nm. No longitudinal spacing is reported since meridional reflections were absent. These values are most similar to those reported by Holland et al., 1.055 and 0.585 nm [23]. Doubling of the unit cell dimensions to accommodate additional peaks has been published for single crystal studies by Klement and Geil [24] and Kumamaru et al. [42], and in these cases could be argued to fit the half [310] plane that is shown in the transmission photograph in Fig. 8 as [1.5 0.5 0]. However, the appearance of this peak in a filament under stress suggests that the distribution of interchain distances narrows with stress, yet this is still associated with emergent order in a disordered or amorphous region. Therefore the overall Paracrystalline-ordered dimensions are unchanged. This behavior does suggest, similar to the crystal–crystal transitions in nylon 66 [43] and poly(vinylidene fluoride) [44], that under more controlled conditions disordered amorphous to ordered paracrystalline transitions are also possible.

Mechanical properties

The PO is shown to be well correlated with mechanical properties of the filaments and their extrusion conditions. Tenacity increases with draw ratio and PO (Fig. 11), with *R*-square values of 0.95 for fiber groups B, including A since it is the first filament in the 100-m min^{-1} (B) group, and 0.50 for groups D, including A since it is the lowest spin-draw filament of the spin-drawn (D) group. Conditions incorporating maximum hot-draw imparted the highest tenacities, while filament drawn at the shroud imparted tenacities that are about one quarter less. Tenacity for the MPHAC is well above the value of the commercial fiber Dralon® and as much as twice as high as general acrylics [45]. Table 3 lists the values of the tensile properties along with the standard deviations. Variations being high at high draw ratios warrant improvement through optimization of the extrusion setup. It is also noted that the tenacity decreases with increase in paracrystal size (Fig. 12). Smaller paracrystals, below 5.0 nm in size, show a tenacity above 3.5 cN $dtex^{-1}$.

Initial modulus (IM) shows less-defined correlation with the PO (Fig. 13). Values for filaments extruded only with spin-draw, sample groups A and D, start at an average of 59 cN $dtex^{-1}$ at 300 m s^{-1} and decrease to just below 44 cN $dtex^{-1}$ at 700 m s^{-1}. IM, however, increases consistently with an increase in hot-draw, sample groups A and B. The highest IM value obtained for the spin-drawn filament (59 cN $dtex^{-1}$) is quite similar to the highest value (54 cN $dtex^{-1}$) obtained with hot roller drawing. The standard deviation for IM is high for spin-drawn filaments and half of those of hot-drawn filaments.

Fiber elongation at break follows a traditional decrease with spin- and hot-drawing (Fig. 14).

It is noted that while the spin- and hot-drawn samples, groups B and D, reach about the same levels of initial moduli, the hot-drawn samples show significantly higher tenacity than the spin-drawn filaments. Since tenacity is

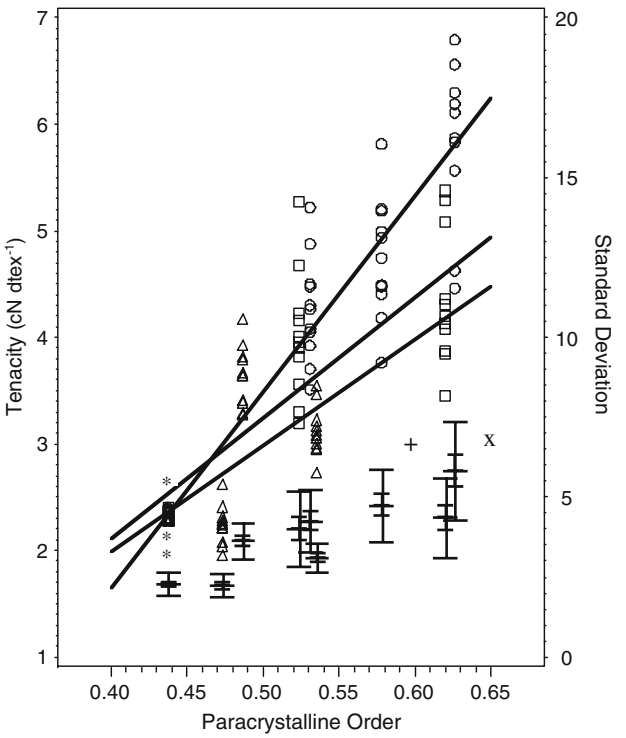

Fig. 11 Tenacity by PO. Filament groups (A) ✳, (B) △, (C) □, (D) ○, Dralon® +, and Orlon® ×

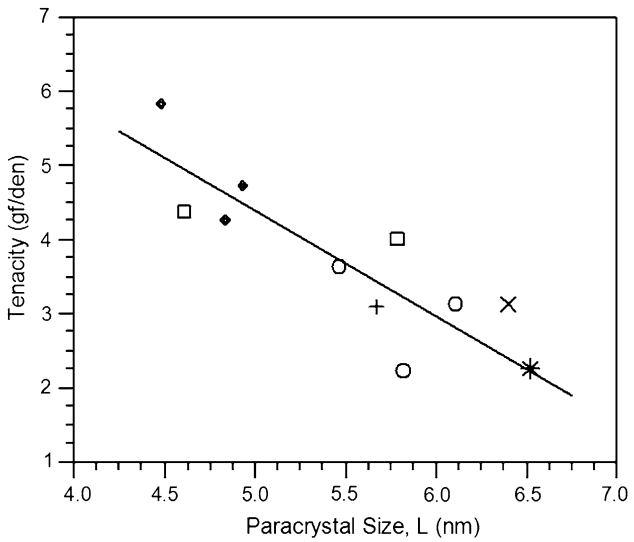

Fig. 12 Average tenacity and paracrystal size. (A) ✳, (B) ◆, (C) □ and (D) ○, Dralon® +, and Orlon® ×

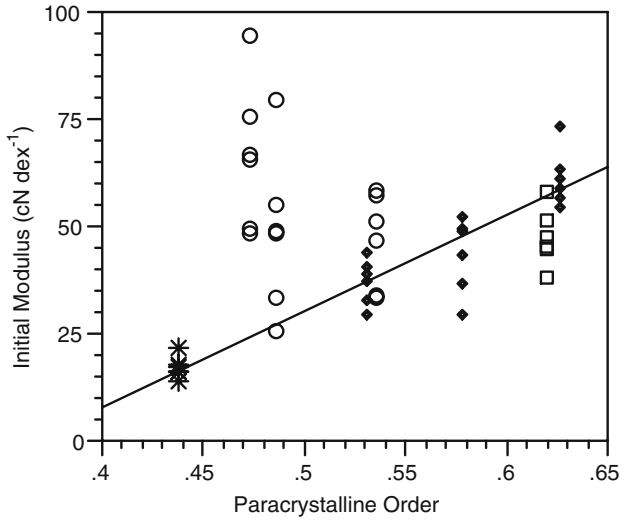

Fig. 13 Initial moduli by PO. (A) ✳, (B) ◆, (C) □ and (D) ○

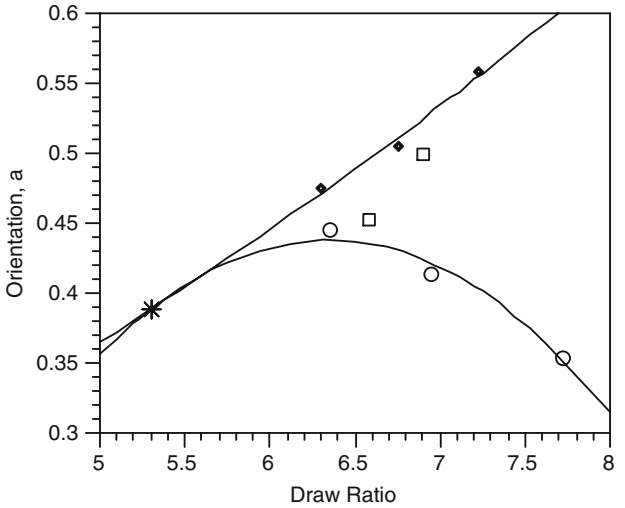

Fig. 15 α-Orientation and draw ratio. (A) ✳, (B) ◆, (C) □ and (D) ○

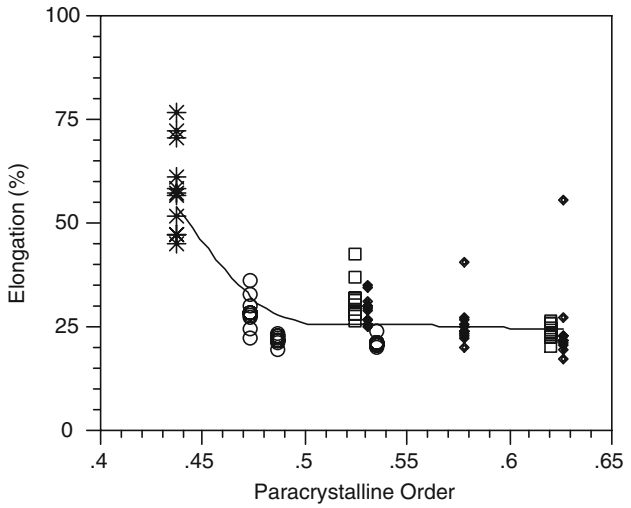

Fig. 14 Elongation by PO. (A) ✳, (B) ◆, (C) □ and (D) ○

influenced by defects, these results may indicate that hot roller drawing develops a more uniform structure along the length of the filament. Filament to filament differences may still be present (high standard deviation), but within each filament of hot-drawn specimens, the structure may be more regular.

Molecular orientation

Generally, axial molecular orientation in filaments of semi-crystalline vinyl polymers directly affects their tenacity and modulus. In these conventional cases, the chains tend to orient parallel to the fiber axis in varying degrees depending on whether the domain is amorphous or crystalline. In many linear polymers, the degree of orientation can be indicated by the magnitude of the observed birefringence. In polymers such as PAN, however, the highly polar and polarizable AN C≡N triple-bonds have as large an influence or larger on induced polarization in the electronic structure of bonds in the perpendicular direction as do the carbon–carbon bonds in the parallel direction [45]. Furthermore, as PAN chains conform in helical rods in the longitudinal direction [7, 21], the birefringence tends to be negligible, or even negative. In such polymers, therefore, the magnitude of birefringence, or the value of the Hermann's Orientation Function, are not effective means of characterizing molecular orientation.

An alternative method of determining orientation in acrylic polymers is the measurement of the α-orientation [35]. The speed at which sonic waves travel along a filament and its sonic modulus is related to the axial molecular orientation (Fig. 15). For filament groups A and B, α-orientation or sonic modulus increases directly with draw ratio. For group D fibers, however, α-orientation or sonic modulus reaches an optimum value and then decreases as draw ratios increase. This difference in behavior and the corresponding mechanical properties suggests that the changes taking place in the structure as a result of these two drawing procedures are different.

Discussion

Melt behavior and copolymer sequence structure

Most high-AN, traditional, or 'flooded,' free-radical PAN homo- and copolymers are known not to exhibit a melting endotherm at low heating rates in a DSC [3, 4, 46]. Eby [16] proposed a method of predicting melting temperatures for copolymers that includes comonomers as defects in

their (para)crystalline regions, and which Frushour [47–50] demonstrated is generally applicable to free-radical AN-copolymers. Inference of a 'melting' point was made from wet, high-pressure DSC scans when mixing two parts water to one part copolymer. For many co- and terpolymers of AN, Eby's model in association with Frushour's wet-point depression accurately predict some type of endothermic behavior for PAN. Yet extrapolating these observations to predict the dry behavior for all common comonomers was not successful.

Frushour's model describing 'melting' behavior for copolymers is dependent on the comonomer concentration and the molar volume of their sidegroups. MA and VA have similar molar volumes, 36 and 39 cm^3 mol^{-1}, respectively. No dry-polymer 'melting' point depression constant is reported for PAN copolymers, including those with MA, as "many of the polymers decomposed before the melting could be measured." Yet for VA, Frushour reports a different wet 'melting' point depression constant than that observed by Slade in dry 'melting' experiments, the former of which is similar to the wet-polymer constant for MA [51]. Since a dry 'melting' temperature depression constant was observed for VA and not for MA comonomers, another aspect of copolymer structure must affect their 'melting' behavior.

While the molar volume of the monomers MA and VA are similar, their reactivity ratios with AN are significantly different. When comparing the predicted and observed AN sequence lengths with respective comonomers, the VA copolymer shows a more alternating and less blocky structure. The second-order Markov (Penultimate) model also more accurately describes the sequence lengths for AN/VA. However, observed molar compositions are only 61, 64, and 75% AN (Fig. 4). The Terminal model predicts a somewhat longer sequence length in both MA and VA copolymers. When comparing the respective predicted AN sequence lengths, the length for the MA copolymer is over two times larger than for the VA copolymer at the same molar compositions. This longer sequence length would provide longer runs of the '(para)crystallizable' AN units and could explain the difference in melting behavior that is observed in these copolymers, and would further address why shrinkage is more prevalent in some AN copolymers at higher comonomer concentrations [35, 52, 53]. Insertion of MA and VA units into PAN likely increases the conformational flexibility of the copolymer relative to PAN homopolymer [54, 55]. This increase in flexibility would be greater in AN/VA copolymers, because the VA units are more randomly inserted compared to the more blocky insertion of MA units. As a consequence, for the same comonomer content AN/VA copolymers would be expected to exhibit higher changes in entropy with shrinkage [35] at lower temperatures.

Differential scanning calorimetry

When considering the MPHAC and its equivalent flooded free-radical copolymer, the larger (para)crystals in the former would normally be expected to be more stable and require a higher melting temperature compared to the usual free-radical PAN copolymers. However, the lack of a discrete melting endotherm probably means that the PAN (para)crystals in the MPHAC are "nonequilibrium," where segmental dipole interactions dominate the usual combination of related torsional, steric, and/or angular constraints on the individual copolymer chains. Since the AN sidegroups have such strong dipole moments, the strength of their interchain interactions supercedes the forces that usually govern the equilibrium conformations of a regular vinyl chain. As such, the disordering of these (para)crystal units may be a transient process and not a first-order thermodynamic transition, whereby increased thermal energy gradually disrupts individual dipole attractions sufficient for melt-processing below the onset of AN degradation. Since the melting thermogram shows no discrete endotherm, the 'as-(para)crystallized' polymer likely transitions from a more nonequilibrium (para)crystal into a less nonequilibrium structure with increased heating. Furthermore, at a heating rate of 5 °C min^{-1} MPHAC-B4 (Fig. 5) shows no glass transition or melting endotherm, which indicates that the "218 °C inflection" observed at higher heating rates likely occurs over a discrete and measurable amount of time, i.e., is not a first-order phase transition typical of the melting of semi-crystalline polymers.

Whatever forms of PO exist in MPHAC, the amount of energy required to decouple the chains or is released when they are recoupled, should be quantifiable and related to the index of paracrystallinity (IP). The amount of energy obtained, especially after repeated cycles of heating and cooling, would be dependent on the mechanisms that drive the dissociation and solidification of PAN chains in the solid state. Since the process of transition from a solid to a 'melt' in the MPHAC is dependent upon time and temperature, this process is likely driven both by thermodynamic and kinetic factors.

Load-elongation curves

In polypropylene and other flexible chain vinyl polymers, lamellae generally form perpendicular to the extrudate axis. The process of drawing induces a necking zone where the local temperature developed in the solid due to deformational hysteresis exceeds the glass transition. This enables the chains to deform and reorient more parallel to the direction of stretch [41]. In the filaments of the MPHAC, a distinct necking zone is absent, but a change in the color of the filament is noted when drawn. The

mechanism of chain deformation is often related to an increase in temperature above the glass transition in local regions as the filament is drawn to allow the side groups to decouple. Upon drawing, the chains are able to pack more regularly in rods. Whether or not they are in helical conformations, their angle with draw will decrease. Accordingly, the PO could be expected to increase with drawing and this is observed in the filaments under study (Fig. 8).

Paracrystalline order

The actual shapes of WAXS spectra for PAN homo- and copolymers vary with chemistry and form of the bulk material [13, 25, 31, 56]. A distinct peak is usually found at $2\theta \approx 17.3°$ along with non-ordered scattering. Occasionally this is accompanied by a smaller peak at $2\theta \approx 29.8°$, whose existence may be further dependent upon tacticity, processing, and comonomer content. In studies of homopolymer PAN lamellae by Holland et al. [23], Klement and Giel [24], and Kumaramu et al. [42], WAXS spectra are notably absent and hinder an analysis of universal crystalline parameters when PAN powder or fibers samples show only two distinct peaks, while lamellae show occasional distant reflections. Given the variations in the placement, position and intensity of peaks, and the nature of the solid-state conformation of PAN chains, a more flexible method is needed to calculate PO.

Gupta et al. presented the most recent procedure for calculating the DO in PAN homo- and copolymers. They characterized the profile in terms of two crystalline peaks: one at $2\theta \approx 17.3°$ and the other at 29.8° and an 'amorphous-scatter' in-between [31]. However, they exclude any calculations of or reference to Miller Indices. Calculating order using only three peaks is unable to account for varying spectra. Spectra collected for the MPHAC, Orlon®, and Dralon® show non-trivial scatter centered between $2\theta \approx 12.9$ and 14.3°, which would be excluded using the Gupta et al. method. To account for this scatter, additional peaks were used here, while the peaks that represent order are $2\theta \approx 17.3$ and 29.8° (Fig. 5). Absent is the broad diffuse scatter reported for typical commercial fibers and copolymer resin. Since a single scattering peak does not correspond to the shape of this spectrum, two peaks are used to fit this area.

The relative shape and intensity of these characteristic peaks were confirmed through simulations by Hobson and Windle [11]. Their work also shows that the order of the [110] and [200] planes, which correspond with the $2\theta \approx 17.3°$ peak, changes with stereoregularity. The spacing between these peaks, however, is generally small and often overlapped, especially for atactic PAN. This form predominates in most acrylics and is observed in MPHAC-B4. The $2\theta \approx 17.3°$ peak is a combination of intensities resulting from planes that correspond with coexisting stereoregularities.

Index of paracrystallinity (IP) and draw ratio

The differences in PO depending on where the draw is imparted, suggest there are different mechanisms driving the solid-state chain conformations. As the solid-state conformation is a function of the dipole interaction and likely irregular and helical, it is difficult to infer with certainty how the degree of intermolecular interaction changes within these limits of draw conditions. Clearly, though, the two zones where draw is imparted differ by temperature. Spin-draw is molten and hot-draw is above the glass transition, and this could have different effects on chain mobility. With hot-draw, there is insufficient thermal energy to completely de-couple the sidegroup interactions to the degree required for melt-processability. Packed helical chains would then extend concurrently with draw. With sufficient thermal energy, neighboring sidegroups could reposition themselves to minimize their inter-chain repulsion, thereby forming more ordered regions.

Mechanical properties

Tenacities of semi-crystalline filament-forming polymers that are useful in consumer and industrial applications become inversely proportional to crystallinity beyond specific values. Mechanical properties, particularly tenacity, deteriorate at higher threshold values of crystallinity [41, 45]. MPHAC resins, however, show a different behavior at the draw ratios investigated. Tenacities as a function of PO were plotted and a linear regression is fitted for fiber groups A and B (Fig. 10). In these cases, the tenacity is highly correlated with the degree of order present. Groups C and D show a similar trend, although with a lower degree of correlation.

The Dralon® fiber shows a relatively high IP, but lower tenacity than does MPHAC. Since PO is presumably driven by the interaction between dipoles, an AN sequence length of approximately 36 in Dralon®, as opposed to 13 in the MPHAC filament, leads to high PO in these fibers. But because the side chain dipolar interactions are so strong, the plastic deformation behavior is not possible in Dralon®. This is, however, not the case for MPHAC with reduced AN block lengths that lead to relatively higher orientation through hot-drawing.

Paracrystal size

In most thermoplastic semi-crystalline materials that form filaments, the crystal size is also correlated to mechanical

properties, such as tenacity. The dependency of these properties stems from the occurrence of weak links in the structure. Larger crystals could cause lower overall tenacities as their presence leads to uneven concentration of loads across the microstructure with the concentration of stress at the boundary of the paracrystal. The load is supported by fewer local domains of chains between crystals, requiring a greater contribution of fewer boundaries, each then having to support a larger load. Paracrystals that are smaller and more abundantly and uniformly distributed allow the load to be shared more evenly and between more chains. This is observed in acrylic fibers, both solution-spun Dralon® and the MPHAC (Fig. 11).

Unit cell parameters

Directly related to the unit dimensions, *d*-spacings for traditional copolymers of AN with methacrylonitrile [31] and MA [28] were shown to change slightly with increasing content of the comonomer. Significant changes were observed at AN contents below 85%, or in the modacrylic region. With respect to MPHAC-B4, an increase of 0.05 nm in the '*a*' dimension could be caused by the pervaded volume of the MA comonomer. This suggests that the unit cell size itself may contribute to the ability of the AN sidegroups in the MPHAC to decouple before degradation. NMR and DSC results indicate that an intermediate number average sequence length of AN units destabilizes the PO sufficiently to enable melt-processability ,while retaining sufficient length for end-use mechanical integrity [29]. Both the unit cell size, as determined by the comonomer's pervaded volume, and the number average sequence length, as determined by the comonomer's concentration and spacing, support melt-processability for MPHAC copolymers.

Recrystallization

Since the melting thermograms of the MPHAC are highly dependent on their ramp rate, where rates below 5 °C min^{-1} show effectively no change in baseline, but at rates of 10 and 20 °C min^{-1} show steadily larger and more distinct peaks. Any semblance of a 'melting' peak in this acrylic disappears with lower heating rates. Many semi-crystalline polymers exhibit similar behavior, where a recrystallization exotherm upon heating can be nonexistent after cooling with a slow enough rate. Additional studies of the thermodynamic and kinetic factors affecting the disassociation and recrystallization of the paracrystal order, such as modulated DSC at ramp rates of 20 °C min^{-1}, may assist in distinguishing between which factors or more important in this system.

Conclusions

The present investigation provides a microstructural basis for the difference in bulk behavior between PAN copolymers produced in scavenged emulsion and flooded copolymerizations, because the AN run-lengths in PAN copolymers produced during scavenged emulsion copolymerization are significantly shorter. This intermediate intrachain microstructure supports a (para)crystalline order in the solid that is able to be disrupted and 'melts' at a lower temperature, rendering it melt-processable. Most importantly, this intermediate average AN sequence length is sufficient to impart mechanical stability by preventing significant shrinkage upon heating. The (para)crystalline domains 'melt' in a nonequilibrium fashion, and indicate that PAN copolymer (para)crystals generally conform in a mesomorphic manner that exhibits no equilibrium first-order phase transition, unlike most semi-crystalline vinyl homo- and copolymers.

Filaments extruded from one version of a melt-processable high-acrylonitrile copolymer (MPHAC-B4) exhibit behaviors from plastic deformation to deformation strengthening during load elongation. Filament with low initial draw shows a pronounced plastic deformation and elongation, while filament drawn to higher ratios shows the type of deformation-strengthening behavior that is expected of traditional acrylic. An IP is calculated from WAXS based on equatorial reflections utilizing additional curves to fit scatter. The PO increases with draw ratio, while hot godet draw imparts a significantly higher degree of PO. Likewise, tenacity and the IP are similarly related, where lower tenacity is related with higher spin-draw and higher tenacity with hot godet draw. Modulus is shown to be directly related to the IP. Elongation is shown to decrease as draw ratio increases. This indicates that the solid-state conformations and mechanics of chain deformation of the melt-processable acrylic are different than both traditional acrylics and vinyl polymers. Sonic modulus shows that a higher molecular orientation is achieved with hot godet draw, rather than spin draw. The IP is shown to be inversely proportional to the paracrystal size. Unit cell dimensions are found to be $a = 1.097 \pm 0.002$ nm and $b = 0.585 \pm 0.004$ nm, and, similar to previous reports, are invariable with draw, but affected by the presence of the comonomer. While a heating endotherm is absent, cooling exotherms disappear with lower ramp rate, indicating that the process of reordering has a kinetic component that predominates at lower cooling rates. The reordering enthalpy, a measure of the cooling exotherm, is shown to be inversely correlated with the IP, but directly correlated with paracrystal size. Finally, no significant changes in molecular weights were observed between initial MPHAC resin pellets and "melt"-processed filaments.

Acknowledgement The Institute of Textile Technology in Raleigh, NC is gratefully acknowledged for research funding.

References

1. Frushour B, Knorr R (1985) In: Lewin M, Pearce E (eds) Handbook of fiber chemistry, vol 4. Marcel Dekker, New York
2. Wade B, Knorr R (1985) In: Masson J (ed) Acrylic fiber technology and applications. Marcel Dekker, New York
3. Dunn P, Ennis B (1970) J Appl Polym Sci 14:1795. doi:10.1002/app.1970.070140713
4. Korte S (1999) In: Brandrup J, Emmergut E, Grulke E (eds) Polymer handbook. John Wiley, New York
5. Mandelkern L (2002) Crystallization of polymers, vol 1. Cambridge University Press, Cambridge
6. Lindenmeyer P, Hosemann R (1963) J Appl Phys 34:42. doi:10.1063/1.1729086
7. Bohn C, Schaefgen J, Statton W (1961) J Polym Sci 55:531. doi:10.1002/pol.1961.1205516212
8. Yamadera R, Murano M (1967) J Polym Sci A 5:1059. doi:10.1002/pol.1967.150050511
9. Bajaj P, Padmanaban M, Gandhi R (1985) Polymer (Guildf) 26:391. doi:10.1016/0032-3861(85)90200-9
10. Schaefer J (1971) Macromolecules 4:105. doi:10.1021/ma60019a022
11. Hobson R, Windle A (1993) Polymer (Guildf) 34:3582. doi:10.1016/0032-3861(93)90041-8
12. Minagawa M, Ute K, Kitayama T et al (1994) Macromolecules 27:3669. doi:10.1021/ma00091a032
13. Minagawa M, Taira T, Yabuta Y et al (2001) Macromolecules 34:3679. doi:10.1021/ma002173e
14. Lee L, Register R (2005) Macromolecules 38:1216. doi:10.1021/ma048013a
15. Flory P (1958) J Trans Faraday Soc 51:848. doi:10.1039/tf9555100848
16. Eby R (1963) J Appl Phys 34:2442. doi:10.1063/1.1702763
17. Flory P (1949) J Chem Phys 17:223. doi:10.1063/1.1747230
18. Lewis F, Mayo F, Hulse W (1945) J Am Chem Soc 67:1701. doi:10.1021/ja01226a025
19. Smierciak R, Wardlow E, Lawrence B (1997) US Patent 5 602 222
20. Dimitratos J, El-Aasser M, Georgakis C et al (1990) J Appl Polym Sci 40:1005. doi:10.1002/app.1990.070400533
21. Henrici-Olive G, Olive S (1979) Adv Polym Sci 32:128
22. Holland V (1960) J Polym Sci XLIII:572. doi:10.1002/pol.1960.1204314229
23. Holland V, Lindenmeyer P, Mitchell S et al (1962) J Polym Sci 62:145. doi:10.1002/pol.1962.1206217310
24. Klement J, Geil P (1968) J Polym Sci A-2 6:1381
25. Hinrichsen V (1972) J Polym Sci C 38:303
26. Joh Y (1979) J Polym Sci A-1 17:4051
27. Kulshreshtha A, Garg V, Sharma Y et al (1986) J Appl Polym Sci 31:1413. doi:10.1002/app.1986.070310525
28. Grobelny J, Sokol M, Turska E (1989) Polymer (Guildf) 30:1187. doi:10.1016/0032-3861(89)90035-9
29. Hutchinson S (2005) M.S. Thesis, North Carolina State University, Raleigh NC, USA
30. Odian G (2004) Principles of polymerization. Wiley-Interscience, Hoboken, NJ
31. Gupta A, Singhal R, Bajaj P (1983) J Appl Polym Sci 28:1167. doi:10.1002/app.1983.070280322
32. Stefani R, Chevreton M, Garnier M et al (1960) Compt Rend 251:2174
33. Colvin B (1974) Eur Polym J 10:337. doi:10.1016/0014-3057(74)90147-5
34. Moseley W (1960) J Appl Polym Sci III:266. doi:10.1002/app.1960.070030902
35. Henrici-Olive G, Olive S, Frushour B (1986) Makromol Chem 187:1801. doi:10.1002/macp.1986.021870723
36. Azuma C, Dias M, Mano E (1995) Polym Bull 34:593. doi:10.1007/BF00423356
37. Brar A, Sunita (1991) In: Sivaram S (ed) Polymer science, vol 2. Tata McGraw-Hill, New Delhi
38. Brar A, Sunita (1992) J Polym Sci A 30:2549. doi:10.1002/pola.1992.080301209
39. Bunsell A, Hearle J, Konopasek L et al (1974) J Appl Polym Sci 18:2229. doi:10.1002/app.1974.070180802
40. Xue T, McKinney M, Wilkie C (1997) Polym Degrad Stabil 58:193. doi:10.1016/S0141-3910(97)00048-7
41. Ward I (1997) In: Ward I (ed) Structure and properties of oriented polymers. Chapman & Hall, London
42. Kumamaru F, Kajiyama T, Takayanagi M (1980) J Cryst Growth 48:202. doi:10.1016/0022-0248(80)90210-9
43. Mehta R (1999) In: Brandrup J, Immergut E, Grulke E (eds) Polymer handbook. John Wiley, New York
44. Kerbow D, Sperati C (1999) In: Brandrup J, Immergut E, Grulke E (eds) Polymer handbook. John Wiley, New York
45. Morton W, Hearle J (1993) Physical properties of textile fibers. Textile Institute, Manchester
46. Hinrichsen V (1971) Angew Makromol Chem 285:121
47. Frushour B (1981) Polym Bull 4:305. doi:10.1007/BF00255108
48. Frushour B (1982) Polym Bull 7:1. doi:10.1007/BF00264150
49. Frushour B (1984) Polym Bull 11:375. doi:10.1007/BF00254277
50. Frushour B (1980) Bull Am Phys Soc 25:352
51. Slade P (1970) Therm Acta 1:459. doi:10.1016/0040-6031(70)85016-X
52. Falkai V (1995) In: Masson J (ed) Acrylic fiber technology and applications. Marcel Dekker, New York
53. Lauterberg W, Kimmer W, Schmolke R (1968) Deu Textiltech 18:657
54. Tonelli A (1974) Macromolecules 10:716. doi:10.1021/ma60057a048
55. Tonelli A (1977) Macromolecules 7:632. doi:10.1021/ma60041a017
56. Frushour B (1995) In: Masson J (ed) Acrylic fiber technology and applications. Marcel Dekker, New York